SANDIA REPORT

SAND2008-6387
Unlimited Release
Printed September 2008

Tritium Storage Material

Donald F. Cowgill, David B. Robinson, Stephen J. Fares, Markus D. Ong, Ilke Arslan, Kim L. Tran, Kevin F. McCarty, George B. Sartor, Kenneth D. Stewart, W. Miles Clift, Weifang Luo, John Smugeresky

Prepared by
Sandia National Laboratories
Albuquerque, New Mexico 87185 and Livermore, California 94550

Sandia is a multiprogram laboratory operated by Sandia Corporation,
a Lockheed Martin Company, for the United States Department of Energy's
National Nuclear Security Administration under Contract DE-AC04-94AL85000.

Approved for public release; further dissemination unlimited.

Issued by Sandia National Laboratories, operated for the United States Department of Energy by Sandia Corporation.

NOTICE: This report was prepared as an account of work sponsored by an agency of the United States Government. Neither the United States Government, nor any agency thereof, nor any of their employees, nor any of their contractors, subcontractors, or their employees, make any warranty, express or implied, or assume any legal liability or responsibility for the accuracy, completeness, or usefulness of any information, apparatus, product, or process disclosed, or represent that its use would not infringe privately owned rights. Reference herein to any specific commercial product, process, or service by trade name, trademark, manufacturer, or otherwise, does not necessarily constitute or imply its endorsement, recommendation, or favoring by the United States Government, any agency thereof, or any of their contractors or subcontractors. The views and opinions expressed herein do not necessarily state or reflect those of the United States Government, any agency thereof, or any of their contractors.

Printed in the United States of America. This report has been reproduced directly from the best available copy.

Available to DOE and DOE contractors from
U.S. Department of Energy
Office of Scientific and Technical Information
P.O. Box 62
Oak Ridge, TN 37831

Telephone: (865) 576-8401
Facsimile: (865) 576-5728
E-Mail: reports@adonis.osti.gov
Online ordering: http://www.osti.gov/bridge

Available to the public from
U.S. Department of Commerce
National Technical Information Service
5285 Port Royal Rd.
Springfield, VA 22161

Telephone: (800) 553-6847
Facsimile: (703) 605-6900
E-Mail: orders@ntis.fedworld.gov
Online order: http://www.ntis.gov/help/ordermethods.asp?loc=7-4-0#online

SAND2008-6387
Unlimited Release
September 2008

Tritium Storage Material

Donald F. Cowgill, Weifang Luo, John Smugeresky
Hydrogen and Metallurgical Science Department

David B. Robinson, Stephen J. Fares, Markus D. Ong, Ilke Arslan, Kim L. Tran
Energy Systems Department

Kevin F. McCarty
Materials Physics Department

George B. Sartor
Thermal/Fluid Science & Engineering

Kenneth D. Stewart, W. Miles Clift
Engineered Materials Department
Sandia National Laboratories
Livermore, California 94550

Abstract

Nano-structured palladium is examined as a tritium storage material with the potential to release beta-decay-generated helium at the generation rate, thereby mitigating the aging effects produced by enlarging He bubbles. Helium retention in proposed structures is modeled by adapting the Sandia Bubble Evolution model to nano-dimensional material. The model shows that even with ligament dimensions of 6-12 nm, elevated temperatures will be required for low He retention. Two nanomaterial synthesis pathways were explored: de-alloying and surfactant templating. For de-alloying, PdAg alloys with piranha etchants appeared likely to generate the desired morphology with some additional development effort. Nano-structured 50 nm Pd particles with 2-3 mn pores were successfully produced by surfactant templating using PdCl salts and an oligo(ethylene oxide) hexadecyl ether surfactant. Tests were performed on this material to investigate processes for removing residual pore fluids and to examine the thermal stability of pores. A tritium manifold was fabricated to measure the early He release behavior of this and Pd black material and is installed in the Tritium Science Station glove box at LLNL. Pressure-composition isotherms and particle sizes of a comercial Pd black were measured.

Acknowledgements

The authors are indebted to Sandia colleagues for their support of this research, particularly to P. Spence, S. Rice, and S. Griffiths for their strong, continued interest. This work was performed under the Laboratory-Directed Research and Development program at Sandia National Laboratories, a multiprogram laboratory operated by Sandia Corporation, a Lockheed Martin Company, for the United States Department of Energy's National Nuclear Security Administration under contract DE-AC04-94AL85000.

Contents

List of Figures

Tritium Storage Material

1. Introduction

In applications where tritium must be used, extremely reliable storage systems involving minimal human intervention are required. The lifetime of compact, solid storage of tritium is currently limited by the effects of the decay product. Beta decay of tritium (T) generates helium-3 at a rate of 0.056 He/T per year. Short-term tritium storage within a bulk metal tritide sequesters much of this He within high-pressure nanometer-scale bubbles, which remain stable to temperatures near the melting point of the metal, i.e., well beyond that needed for desorbing the tritium. The useful life of this He-free tritium storage is limited by the He bubble growth with time. When the He concentration within the metal tritide (He/M) reaches a critical value, the bubbles become unstable and He is rapidly released from the solid. The highest known critical He/M occurs in bulk Pd tritide and is about 0.5 He/Pd [Emig 92]. When stored in a tritium-replenishing overpressure, bulk $PdT_{.6}$ begins releasing He at 1-2 times the generation rate at about 14 years, and somewhat earlier for small dimension materials. For longer-term storage of He-free tritium, a new approach is needed.

Prior Sandia work has demonstrated that few helium bubbles form within a few nanometers of the solid surface: helium is able to escape from this region without nucleating bubbles [Thomas 83]. We seek to build on this discovery, to develop a thorough understanding of the phenomenon, and to use that understanding to design next-generation tritium storage systems. This LDRD project is the first step toward this goal. This report documents efforts to map the helium escape effect as a function of temperature and material geometry, and to refine our models of the process [Cowgill 04-06]. It summarizes initial work to synthesize nanoporous storage materials in which all points within the solid are within a few nanometers of a surface in accordance with the refined model. It also describes a new tritium manifold, fabricated to measure the Early He Release Fraction (ERF) of materials and currently installed in the new Tritium Science Station (TSS) glove box at LLNL. This report will provide guidance toward the next step in reaching the goal of a long-term, He-free tritium storage material.

References

D.F. Cowgill, Sandia Technical Reports SAND2004-1739 and SAND2006-7779; J. Fusion Sci. and Technol. **48**, 539 (2005).

J.A. Emig, R.G. Garza, L.D. Christensen, P.R. Coronado, P.C. Souers, J. Nucl. Materials **187**, 209 (1992).

G.J. Thomas, Radiation Effects **78**, 37 (1983), and private communication.

2. Background

For many years, Sandia has been experimentally and theoretically investigating He trapping and bubble formation within aging metal tritides. We recently generated a model of the bubble evolution, which incorporates much of this information [Cowgill 04-06]. The model includes modules on bubble nucleation, growth, linkage, and finally linked-network percolation and rapid He release. Nucleation has contributions from He self-trapping (trapping within the lattice strain field of another He) and trapping at intrinsic void-type defects and includes parameters derived from atomistic modeling [Baskes 83]. It accounts for bubble densities and bubble characteristics in aging Pd tritides, as well as effects on the Pd lattice. It shows that under certain conditions, He generated within nanoporous or thin film material will have a high probability of escaping through a surface before nucleating a bubble. These conditions are those that provide it with a low probability of encountering another He: an enhanced diffusion rate relative to the generation rate and a short path to the surface.

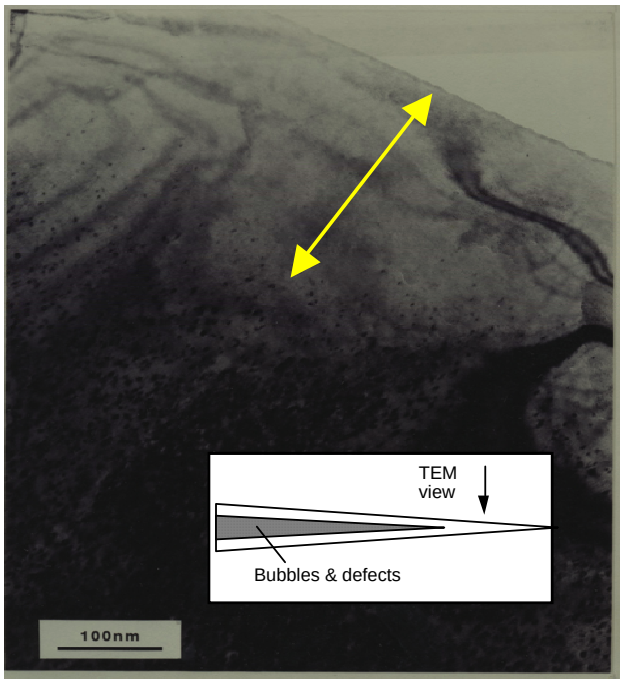

Figure 2.1. Bubble denuded zone at edge of wedge-shaped PdT_x foil [Thomas 83].

Additional support for the idea that nanostructured material will retain little helium comes from TEM observation [Thomas 83] of bubble-denuded zones (about 10 nm thick) near surfaces. (Fig. 2.1) These interfaces provide He sinks that reduce the mobile He concentration and bubble nucleation. There also exists some data on early-stage He evolution from nano-particulate Pd and U tritides [Malinowski 78] that shows much of the He generated in nano-textured Pd black is released rather than retained. This data is compared with model calculations in Sec. 3. The uranium data show that multiply-processed (re-tritided) material releases more He at an early age

than singly-processed UT_3. It is known that this material becomes more finely-divided with such processing. However, experience with the U-beds commonly used in tritium work also shows that even after many cycles, some He retained in the bed is delivered along with the tritium when the bed is heated to about 400°C.

Major improvements have been made in the past decade toward the development of nanoporous metals. Two major approaches have been used: de-alloying and surfactant templating. Nearly all of these have been targeted toward development of other metal systems. Selective dissolution of metallic alloys is a proven route to synthesize nanoporous metals such as gold [Biener 06], copper [Hayes 06], nickel [Sun 04], and platinum [Pugh 03] with remarkable properties. The best-studied material, nanoporous gold, is typically produced by dissolving silver from Ag-Au alloys using nitric acid. The result is an open, three-dimensional pore structure with uniform ligaments, as small as 10 nm, controlled by the alloy composition and de-alloying conditions. This approach can produce 30 percent dense monoliths, such as pellets, of nanoporous metal that are stronger than bulk Au. While there are no reports of producing nanoporous Pd by de-alloying, we note that Pd forms solid solutions with Ag in the same fashion as Au, and that Cu and Ga have been selectively dissolved from Pd-Cu-Ga alloys [Sun 02], so this is likely to be a fruitful approach.

Surfactant templating has already been shown to be a successful route to electroplated nanoporous Pd [Elliott 99]. A more scalable route involves electroless plating, where the metal is reduced in bulk rather than at an interface. This was demonstrated for Pd, but with a less relevant surfactant [Lee 06], and for Ni and Co [Yamauchi 04].

References

M.I. Baskes, M.S. Daw, and W.D. Wilson, *Advances in the Mechanics and Physics of Surfaces II*, T.E. Fischer and R.M. Latanision eds., Harwood Acad. Pub., New York, 1983.

J. Biener, A.M. Hodge, J.R. Hayes, C.A. Volkert, L.A. Zepeda-Ruiz, A.V. Hamza, F.F. Abraham, Nano Letters **6**, 2379 (2006).

D.F. Cowgill, Sandia Technical Reports SAND2004-1739 and SAND2006-7779; J. Fusion Sci. and Technol. **48**, 539 (2005).

J. M. Elliott, G. S. Attard, P. N. Bartlett, N. R. B. Coleman, D. A. S. Merckel, and J. R. Owen, Chem. Mater. **11,** 3602 (1999).

J.A. Emig, R.G. Garza, L.D. Christensen, P.R. Coronado, P.C. Souers, J. Nucl. Materials **187**, 209 (1992).

J.R. Hayes, A.M. Hodge, J. Biener, A.V. Hamza, K. Sieradzki, J. Materials Res. **21**, 2611 (2006)

C.-L. Lee, L.-C. Kuo, Y.-C. Huang, and Y.-W. Yen, Electrochem. Comm. **8,** 697 (2006).

M.E. Malinowski and P.R. Coronado, Sandia Nat'l Laboratories, unpublished data (1978).

D.V. Pugh, A. Dursun, S.G. Corcoran, J. Materials Research **18**, 216 (2003).

L. Sun, C.L. Chien, P.C. Searson, Chem. of Materials **16**, 3125 (2004).

D. Sun, P. Monaghan, W.A. Brantley, W.M. Johnston, J. Materials Science, Materials in Medicine **13**, 443 (2002).

G.J. Thomas, Radiation Effects **78**, 37 (1983), and private communication.

Y. Yamauchi, T. Yokoshima, T. Momma, T. Osaka, and K. Kuroda, J. Mater. Chem., 14, 2935 (2004).

3. The Helium Retention Model

The Sandia model of helium Bubble Evolution (SBE) and He retention in palladium tritide [Cowgill 04] was adapted to nano-structured Pd by adding additional terms to the self-trapping module. Bubble nucleation by self-trapping begins with the stochastic formation of He-pairs formed from diffusing He atoms and bound by a pairing energy E_2. Each pair may dissociate or be promoted to a triplet, where each He is bound to the other two by a binding energy E_3. The dissociation and promotion rates depend on temperature and arrival rate of additional He atoms. Similarly, each triplet may dissociate or be promoted to a quad, etc. For nano-material with the large proximity of surface sinks, the He concentration is low and promotion rates are depressed relative to rates bulk material. As a result, the stability of triplets and other low-order clusters becomes important.

Rate equations for He triplets with E_3=.40 eV and quads with E_4= .56 eV [Baskes 83] were added to the code and bubble nucleation was evaluated for several material thicknesses and temperatures. The computed cumulative He release for 12 nm thick $PdT_{.65}$ at 300K is shown in Fig. 3.1. Also plotted are experimental He retention data points for the 9 samples of Pd black (particle size typically 12 nm) examined by Malinowski [Malinowski 78]. The original data has much sample-to-sample scatter; so here, each data point is averaged using a 5-point smoothing routine.

Both the calculated initial rise and the 0-1500 day average retention of 50-60% agree well with the experimental data, lending confidence to the model. Clearly, significant bubble nucleation still occurs for 12 nm material at 300K. Early in life, new bubble nucleation and trapping at existing bubbles produce an increasing He retention. Later, this retention gradually decreases as individual bubbles deeper within the material get large enough to breach the surface. The model calculation for 6 nm material predicts the retention should drop to 10-20% for the finer scale, still somewhat less greater desired.

The computed He retention for longer times at several temperatures is shown in Fig. 3.2. At about 13 years, the retention at 300K decreases abruptly, signaling onset of the rapid release stage. Increasing the material temperature decreases the retention. The calculation shows that for this material a temperature of 500 K is needed to reduce the retention to a few percent over the first few years. In all cases, the abrupt rapid He release stage is prevented only by conditions that generate a sufficiently low bubble concentration so that bubbles breach the surface before becoming interconnected.

References

D.F. Cowgill, Sandia Technical Reports SAND2004-1739 and SAND2006-7779; J. Fusion Sci. and Technol. **48**, 539 (2005).

M.E. Malinowski and P.R. Coronado, Sandia Nat'l Laboratories, unpublished data (1978).

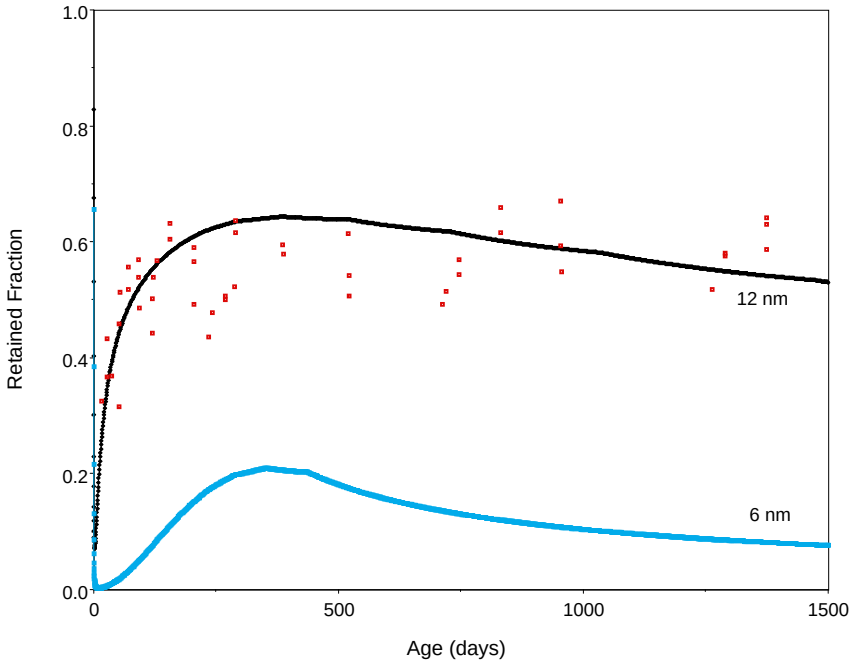

Figure 3.1. Model-computed He retention for 6 and 12 nm Pd at 300K compared with data (red dots) on Pd black [Malinowski 78].

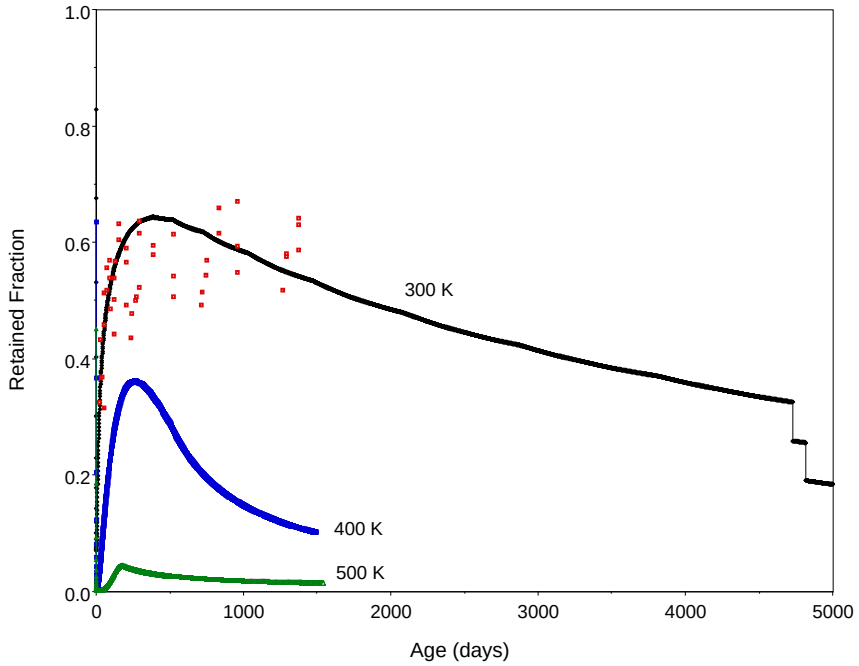

Figure 3.2. Computed long-term He retention behavior for 12 nm Pd at 300, 400, and 500 K.

4. Synthesis of Nanoporous Pd by De-alloying

Selective dissolution of metallic alloys is a proven route to synthesize nanoporous metals such as gold[1], copper[2], nickel[3], and platinum[4] with remarkable properties. Consider the best-studied material, nanoporous gold, which is typically produced by dissolving silver from Ag-Au alloys using nitric acid[1]. An open, three-dimensional pore structure is produced. The ligament dimension, which can be as small as 10 nm, is controlled by the alloy composition and dealloying conditions. The approach can produce monoliths, such as pellets, of nanoporous metal that are surprisingly strong[1]. To our knowledge, nanoporous Pd has not been made from the dealloying approach. The ability to synthesize monoliths of an open pore structure with ligaments about 10 nm wide would be nearly ideal for the He-free storage of hydrogen.

An additional advantage of dealloying is that highly pure material could be produced. That is, the initial alloy can be extremely pure. Even if dealloying does not completely remove the less-noble component of the alloy, the dealloyed material will be free of other contaminants. In contrast, surfactant-based synthesis approaches are prone to contamination by carbonaceous species and salts, which may be difficult to remove, particularly from porous materials.

In this LDRD we explored two different approaches to dealloying: 1) free corrosion and 2) electrochemical dissolution. In free corrosion, an alloy is immersed in a solution that selectively removes one element from the binary alloy. In electrochemical dissolution, the alloy is electrically biased to a potential that selectively oxidizes (dissolves) the less-noble element. In both approaches the electrolytic solution plays a key role. That is, the electrolyte must prevent passivation and allow sufficient surface mobility of more-noble element so that the ligament structure can form. Electrochemical etching offers more control (another "knob") at the price of complexity – the specimen must he electrically contacted and either the current or potential controlled.

4.1. Material Synthesis

Three solid-solution alloys were investigated – Ag-Pd, Ni-Pd, and Cu-Pd. These alloys combinations are perfectly miscible at all compositions. This fact assures that the alloys are spatially homogeneous, a attribute for dealloying. A foil of 70 atomic % Ag and 30% Pd was purchased from Goodfellow Inc. Since no commercial source could be found for the Ni and Cu alloys, they were synthesized in-house by arc melting. High-purity metal shot of the constituent elements were weighed to give alloys with 70 atomic percent of the less-noble element (i.e., Ni and Cu). The pieces were melted together to form a single slug. The slug was then flipped over on the water-cooled hearth and re-melted 4 times, flipping after each melting. The slug was then flattened into a crude foil by mechanical "blacksmithing," that is, by deforming it with a ball-peen hammer. The foils were used with no further processing. The mechanical deformation introduces significant damage (e.g., introducing a high density of dislocations into the foil). Annealing the foils to remove the work damage before dealloying may produce somewhat different results.

In addition to the Ag, Ni, and Cu alloys, we also prepared Si-Pd alloys. The idea was that the large difference in chemical reactivity between Si and Pd would enable a viable free-corrosion

process. Our first effort prepared 60% Si/40% Pd. Based on the phase diagram, this composition is near a eutectic that melts at about 870°C[5]. The hope was that we could quench from the homogenous melt and cool rapidly enough to avoid phase separation. The 60% Si/40% Pd material was sealed in an evacuated fused silica tube and then suspended in a tube furnace. After heating for about 1 hour at 1000°C, the tube was dropped into a bucket of water. Unfortunately, elemental analysis in the SEM showed that phase separation occurred even with the quenching. That is, energy dispersive spectroscopy (EDS) analysis clearly showed two phases, Si-rich and Si-poor. Since the dealloying approach requires a single-phase alloy, the two-phase microstructure of 60% Si/40% Pd precludes this material from dealloying consideration.

Since we were unable to make single-phase 60% Si/40%Pd, we instead synthesized the line compound 50% Si/50% Pd by heating the elements at 1150°C in an evacuated fused silica tube and cooling in the furnace after shutting off the power. While this makes a single-phase compound, ideally in dealloying, the fraction of the less-noble element should be >70%.

4.2. Selection of Etchants for Free-Corrosion

We initially emphasized the simplest approach to dealloying, that of free corrosion. That is, where the alloy is immersed in a solution that might selectively dissolve one of the alloy components. The choice of etchants was based largely on two references. Williams, Gupta, and Wasilik have characterized a large number of etchants for use in micromachining[6]. In particular, they characterize a number of commercial etchants that have been developed for the plating/hybrid circuit industries to selectively etch Cu and Ni from printed circuit boards. The handbook by Walker and Tarn characterizes a large number of etchant/material system combinations[7]. Based on these references, the following etchants were evaluated:

Table 4.1. Descriptions of etchants

Al Etch A: Aluminum etchant type A from Transene: 80% H_3PO_4 + 5% HNO_3 + 5% CH_3COOH + 10% H_2O, typically used at about 50°C
CR-7: Chromium etchant from Cyantek: 9% $(NH_4)_2Ce(NO_3)_6$ + 6% $HClO_4$ + H_2O Known to etch Cu and Ag at useful rates
Known to etch Cu and Ag at useful rates
CE-200: Copper etchant from Transene: 30% $FeCl_3$ + 3-4% HCl + H_2O
APS 100: Copper etchant from Transene: 15-20% $(NH_4)_2S_2O_8$ + H_2O
Piranha: About 50 parts 96% H_2SO_4:1 part 30% H_2O_2, typically used at about 120°C, prepared in house by adding the H_2O_2 to heated H_2SO_4 containing the alloy coupon
$FeNO_3$-$9H_2O$: The salt $FeNO_3$-$9H_2O$ was dissolved in H_2O to varying concentration
NH_4F: NH_4F dissolved in H_2O to 40% concentration

4.3. Electrochemical Dealloying

An additional degree of freedom that can be used in dealloying is to apply a electrical potential to the alloy while in an electrolyte. By adjusting the potential, the dissolution of the less noble alloy element can be enhanced. That is, the difference in the oxidation potentials can be utilized to enhance dealloying. Obviously electrochemical dealloying should become easier as the oxidation/reduction potential between the two elements increases. As Table 4.1 shows, of the three fcc metals tried (Cu, Ni, and Ag), Ni has the largest difference in reduction potential from Pd. The large differences in oxidation/reduction potentials between Pd and the electropositive elements Ga, Zn, Mn, and Si also offer possible approaches to electrochemical dealloying.

Table 4.2. Standard reduction potentials

Source: CRC Handbook of Chemistry and Physics, 67th Edition. p. D-151	
$Au^{+} + e^{-} \Leftrightarrow Au$	1.69 V
$Pd^{+2} + 2e^{-} \Leftrightarrow Pd$	0.951 V
$Ag^{+} + e^{-} \Leftrightarrow Ag$	0.800 V
$Cu^{+} + e^{-} \Leftrightarrow Cu$	0.521 V
$Cu^{+2} + 2e^{-} \Leftrightarrow Cu$	0.342 V
$Ni^{+2} + 2e^{-} \Leftrightarrow Ni$	-0.257 V
$Ga^{+3} + 3e^{-} \Leftrightarrow Ga$	-0.560 V
$Zn^{+2} + 2e^{-} \Leftrightarrow Zn$	-0.762 V
$Mn^{+2} + 2e^{-} \Leftrightarrow Mn$	-1.1.85 V
$SiO_3^{-2} + 3H_2O + 4e^{-} \Leftrightarrow Si + 6OH^{-}$	-1.697 V

An important ingredient of electrochemical dealloying is finding an electrolyte that does not passivate the alloy. That is, if the alloy becomes coated with an oxide, for example, dissolution can be inhibited. We selected the "critical" etching potential[8] by measuring the current as a function of potential, as referenced against an inert, negatively biased counter electrode such as Pd, Au, or Ni.

4.4. Results – Free Corrosion

Tables 4.3-7 summarize the results of the free corrosion approach, along with those of electrochemical corrosion. Overall, the Pd alloys were remarkably hard to dealloy. Typically, the alloys were not attacked or completely (non-selectively dissolved). In particular, the etchants that are designed to remove elemental Cu (CE-200 and APS 100) removed no Cu from the alloy. These results highlight the strong effect that alloying can have on chemical reactivity. Figure 4.1 shows a 70% Ni/30% Pd alloy (Sample 1) that has been etched (likely without dealloying) without forming porosity.

An exception to the typical case of either no corrosion or no selectivity is the case of 70% Ag/30% Pd etched by piranha ($H_2SO_4 + H_2O_2$). As the SEM images in Fig. 4.2 show, a porous structure was achieved. Figure 4.3 shows the uniform starting foil. Elemental analysis in the SEM by energy dispersive spectroscopy (EDS) showed that the porous structure was > 90% Pd.

That is, Ag was selectively removed from the alloy. We note that the reaction (sample 70% Ag/30% Pd S8, Table 4.3) occurred rapidly, that is, in the short time period over which the H_2O_2 was added to the hot H_2SO_4. The dealloying stops as the H_2O_2 decomposes. Crude cross sectional analysis revealed that the entire alloy was not dealloyed. Presumably, etching longer using a configuration that meters H_2O_2 into the solution would allow the complete specimen to be dealloyed.

4.5. Results – Electrochemical Dealloying

Electrochemically etching 70% Ag/30% Pd, 70% Ni/30% Pd, and 70% Cu/30% Pd in 0.5 M perchloric acid yielded essentially no weight loss. Electrochemically etching 70% Cu/30% Pd in CE200 totally dissolved the specimen. However, electrochemically etching 70% Cu/30% Pd in CR-7 led to significant weight loss. (In contrast, free corrosion with CR-7 produced no weight loss.) SEM/EDS analysis to determine if this sample was dealloyed is underway as this report is being written. Electrochemically etching 50% Si/50% Pd in weak HF produced a small weight loss. SEM/EDS analysis to determine if this sample was dealloyed is underway as this report is being written.

4.6. Recommendations

Clearly dealloying can produce nanoporous Pd, as our results dealloying 70% Ag/30% Pd using piranha chemistry show. It is likely a method using piranha could be developed that dealloys the entire thickness of foils or small pellets. The method might involve continually injecting H_2O_2 into an agitated solution, so as to sustain the highly reactive chemistry for sufficient time to etch through the alloy. Clearly there are other free corrosion chemistries to try, including alloys of Pd with chemically dissimilar elements such as Ga, Mn, and Zn. Future effect on solid-solution alloys should investigate annealed alloys where the work damage of plastic deformation has be removed. Finally our efforts devoted to electrochemical etching were limited and many possible combinations of alloys and electrochemistry remain to be explored.

4.7. Dealloying References

1. Size effects on the mechanical behavior of nanoporous Au, Biener, J; Hodge, AM; Hayes, JR; Volkert, CA; Zepeda-Ruiz, LA; Hamza, AV; Abraham, FF, Nano Letters; 2006; v.6, no.10, p.2379-2382.
2. Monolithic nanoporous copper by dealloying Mn-Cu, Hayes, JR; Hodge, AM; Biener, J; Hamza, AV; Sieradzki, K, Journal of Materials Research; 2006; vol.21, no.10, p.2611-16.
3. Fabrication of nanoporous nickel by electrochemical dealloying, Sun, L; Chien, CL; Searson, PC, Chemistry of Materials; 2004; v.16, no.16, p.3125-3129.
4. Formation of nanoporous platinum by selective dissolution of Cu from $Cu_{0.75}Pt_{0.25}$, Pugh, DV; Dursun, A; Corcoran, SG, Journal of Materials Research; 2003; vol.18, no.1, p.216-21.
5. Binary alloy phase diagrams, Edited by T. B. Massalski, (American Society of Metals, Metals Park, OH) 1986.
6. Etch rates for micromachining processing - Part II, Williams, KR; Gupta, K; Wasilik, M, Journal of Microelectromechanical Systems, 2003; v.12 p. 761-778

7. CRC handbook of metal etchants, P. Walker and W. H. Tarn editors (CRC Press, Boca Raton, LA) 1991.
8. Characteristic features of alloy polarization curves, Pickering, H. W., Corrosion Science, 1983, v. 23. No. 10, p. 1107-1120.

Table 4.3. Ag 70%/30% Pd trials

Sample ID	Etchant	Initial Weight (mg)	Post Weight (mg)	Weight Lost (mg)	Etch time	Notes		Comments
Ag70/Pd30 S1	5:1 Nitric Acid	191.6	130.9	60.7	18 hours	Mixed with Di H20 etch orange/gold in color, rinse w/ di H20	Slight dull fininsh non-selective	
Ag70/Pd30 S2	2:1 Nitric Acid	141.6	0	141.6	21 hours	Mixed with Di H20 etch orange/gold in color, rinse w/ di H20	Dissolved sample	
Ag70/Pd30 S3	50:1 Piranha no heat	145.3	141.3	4		Initial reaction some bubbling, sample discolored to gray	some dealloying See SEM images	
Ag70/Pd30 S4	4:1 Piranha 100°C	154.5	151.1	3.4	2 hours	No discoloration in sample	No reaction	
Ag70/Pd30 S5	Cyantec CR-7	145.9	104.6	41.3	22 hours	No reaction, no discoloration	No Dealloying	
Ag70/Pd30 S6	FeNO3-9H2O/ H2O 20	184.1	0	184.1	16 hours	10 grams FeNO3-9H2O dissolved in 10 ml of di H2O	Dissolved sample	
Ag70/Pd30 S7	FeNO3-9H2O/ H2O 20	192.9	192.8	0.1	3.5 hours	5 grams FeNO3-9H2O dissolved in 10 ml of di H2O	No reaction	
Ag70/Pd30 S7.2	FeNO3-9H2O/ H2O 48	192.8	191.7	1.1	2 hours	Heated sample to 48°C	No reaction	
Ag70/Pd30 S8	4:1 H2SO4:H2O2	158	113.1	44.9	10 minutes	Heated H2SO4 ~50°C added sample then added H2O2, Violent reaction, boiling out of bei into secondary container	some dealloying See SEM images	
Ag70/Pd30 S8E	4:1 H2SO4:H2O2	129.1	103.3	25.8	30 minutes	20 ml H2SO4:5m H2O2, heated H2SO4 ~40°C drippped @ ~1 drop/4 sec until reaction was over Intitial reaction none~3 minutes slight bubbling on surface, drops slowed ~6 sec, solution turnes light gold	some dealloying	
Ag70/Pd30 S9	.5M Perchloric Acid, electrochemically etched at ~2.1 mA	302.4	302	0.4	22 hours	Sample still looks shiny, gas is being generated		
Ag70/Pd30 S9A	.5M Perchloric Acid, electrochemically etched at ~18 mA	302	302	0		Increased current significantly Sample still looks shiny, gas is being generated	No reaction	
Ag70/Pd30 S10	2:1 H2SO4:H2O2 20 ml H2SO4:10 ml H2O2 40°C	162	54.5	107.5	3 hrs/10min:	Dripped H2O2 ~1drop/2sec, after 5 ml of H2O2 no reaction. Assumed 40ml beaker to narrow switched to 200ml beaker and flowed H2O2 Quick reaction, violent bubbling ~25 seconds Solution brown/gold, turned off heat sat in solution for 5 additional hours	some reaction See SEM images SEM data to follow	

Table 4.4. Ni 70%/30% Pd trials

Ni70Pd30 S1	2:1 DiH2O: HNO3	118.2	11.1	107.1	2 hours	Initial reaction, none; within 2 minutes yellow discoloration on sample, darkening the sample	some etching, no porosity See SEM images
Ni70Pd30 S2	CR-7 5 ml	124	124	0	504 hours	nothing happened	No reaction
Ni70Pd30 S3	CE-200 5 ml	110.3	6.3	104	18.5 hours	CE200 is brown etchant, dark brown when completed	some etching, no porosity See SEM images
Ni70Pd30 S4	FeNO3-9H2O/ H2O 70 half strength 5gm:10ml diH2O	131.1	130.1	1	4.5 hours	etchant bright orange in color, no initial reaction	No reaction
Ni70Pd30 S5	FeNO3-9H2O/ H2O 70 full Strength 10gm:10ml di H2O	142.8	0	142.8	5 hours	etchant bright orange in color, after 2 hours dark brown, until the end	Dissolved sampe
Ni70Pd30 S4A	.5M Perchloric Acid, electrochemically etched at ~3.1 mA	127.3	117.7	9.6	6.5 hours	sample detached from copper wire	No Dealloying 2.3 V @ 3.1 mA Reference Electrode Ni
Ni70Pd30 S4A	.5M Perchloric Acid, electrochemically etched at ~2.1 mA	117.7	117.6	0.1	12 hours	after 4 hours sample had to lowered into solution incresed current from 2.1 mA to 2.9 mA	No reaction 2.4 V @ 2.1 mA Reference Electrode Ni

Table 4.5. Cu 70%/30% Pd trials

Cu70Pd30 S1	CR-7 5 ml	80.4	80.4	0	120 hours	No reaction, no discoloration	No reaction
Cu70Pd30 S2	APS 100 @ 35°C	199.9	199	0.9	5 hours	Slight bubbling on surface sample discolored to brownish/black after etch	No reaction
Cu70Pd30 S3	CE-200, 5 ml room tem	143.7	51.5	92.2	5 hours	Sample silver in color after etch	
Cu70Pd30 S4	Al etch A @ 40°C 5ml	120	17.7	102.3	6 hours	Initial reaction, yellowing of liquid some bubbling Etchant turned dark brown, final temp 45°C considerable weight lose	Essentially dissolved specimen
Cu70Pd30 S5	.5M Perchloric Acid, electrochemically etched ~4 mA	143.4	142.2	1.2		Redo on Sample 1, weight includes wire Not much happened	No reaction gas evolution 1.2 V @ ~4 mA Reference electrode Ag
Cu70 Pd30 S5	CR-7 5 ml & 200µl HNO @ 35°C	143.9	143.4	0.5	24 hours	No reaction at all	No reaction
Cu70 Pd30 S6	Electrochemical CR-7 20 ml solution	218.5	103.2	115.3	26 hours	Power supply had constant current option set @ 80mA, 2.2 volts 7 am next day added 2ml of CR-7 to submerge sample, sample fizzed entire experiment, darkening aound bottom edge	2.2 volts @ 80mA Significant weight loss SEM data to follow Ref electrode Cu
Cu70 Pd30 S7	Electrochemcal CE200 20 ml solution	174.6	0	174.6	24 hours	(-) Cu lead etched away immediately turning solution black, swithched to Ni lead 2 volts @140 mA Sample spot welded to Ni	sample dissolved

Table 4.6. Si/Pd trials

Si60Pd40 S1	20ml DiH2O:9.954g KC	116.1	102	14.1	3 hours	Initial reaction none, temp 47°C	
	heated to ~75°C					some fizzing ~ 3minutes, 63°C fizzing appears to	
						fragment sample, 9:15 still fizzing temp ~73°C	
				0			
Si50Pd50 S2	20ml DiH2O:10.116g K	83.8	71.8	12	1 week	Heated for 6 hours ~75°C, turned off heat	Weight loss due to sample
	heated to ~75°C					sample weight 74.8mg, added 20 ml Di H2O	crumble
						soaked at RT for 6 days	
Si50Pd50 S3	40% NH4F	65.8	44.8	21	16.5 hours	Immediately brown fizzing from sample	Some reaction
						Solution turned yellow, sample reduced in size	Sample very fragile
						Solution turned more orange than yellow	
Si50Pd50 S4	3% HF: Di H2O	641.1	638.9	2.2	36 hours	Weight includes gold basket	Reference Electrode Au
	40ml DiH2O:			0		Basket has dark purple color, bubbles	1.5 V @ ~ 2.5-2.9 mA
	2.4488 49%HF					forming on basket	SEM data to follow
	electrochemically etched						
	at ~2.5 mA						

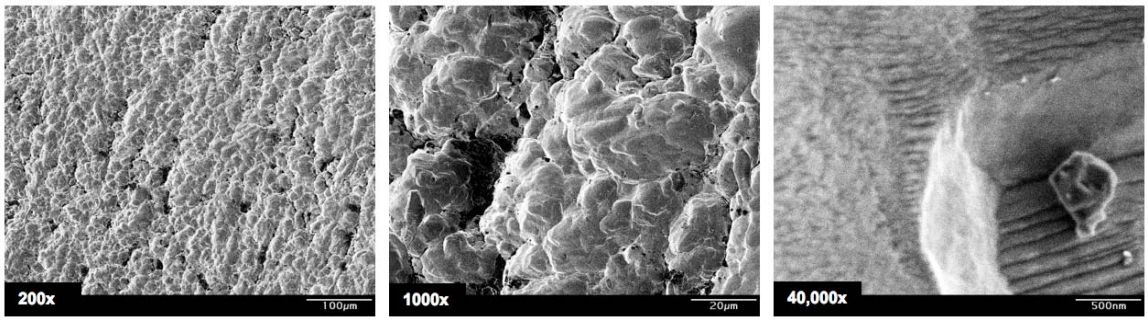

Figure 4.1. SEM images of Ni 70/Pd 30 Sample 1 showing etching without forming a porous material. Likely dealloying did not occur, although this was not confirmed.

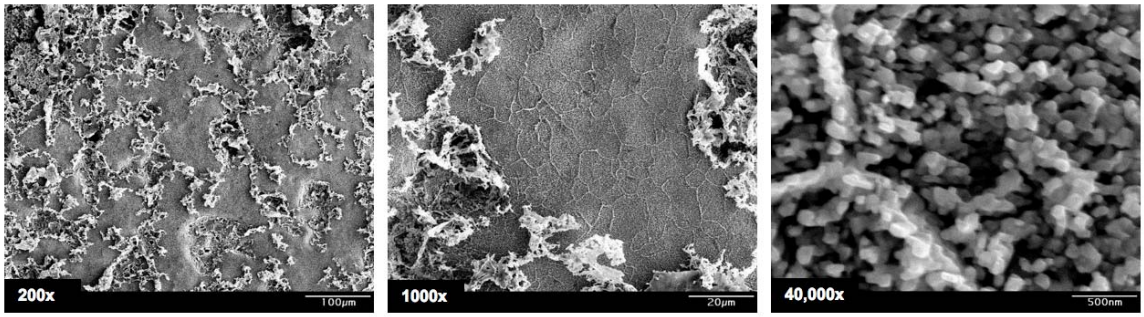

Figure 4.2. SEM images of Ag 70/Pd 30 Sample 8 dealloyed in piranha solution. EDS analysis showed that "lacey" material visible at low magnification (left) and the porous material shown at high magnification (right) consist to 92-95% Pd. That is, Ag was selectively removed from the alloy.

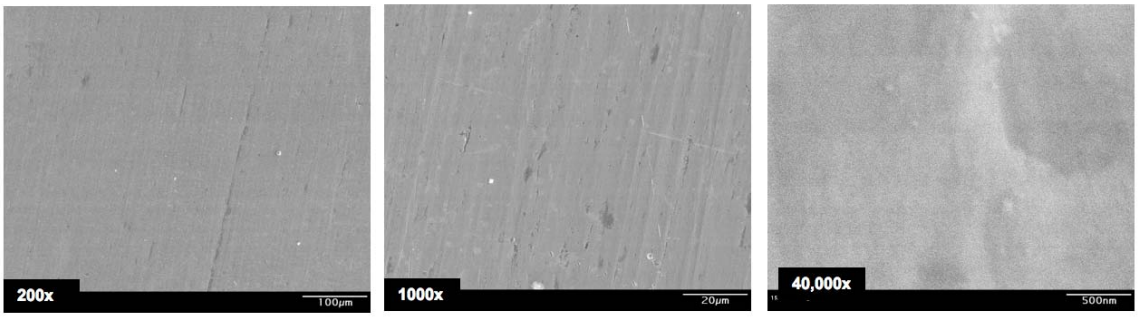

Figure 4.3. SEM images of Ag 70/Pd 30 foil before treatment, showing a uniform, flat surface.

5. Synthesis of Nanomaterial by Surfactant Templating

Palladium and platinum are of well known value for applications in catalysis, hydrogen storage, and electrochemistry.[1] Interfacial interactions can often limit performance, so high surface areas are usually desired. In that case, as a practical maximum, every point in the material would be within a few atoms of an interface. Such materials would exhibit high double-layer capacitance, higher reaction rates in kinetically limited interfacial reactions, and in the case of palladium, rapid charging with hydrogen. Porous platinum and palladium thin films have been fabricated by electrochemical deposition in a surfactant template.[2,3,4,5,6,7] Bulk powders of porous nickel can be formed conveniently through chemical reduction of nickel salts around a surfactant template.[8,9,10] Other relevant methods include assembly of nanoparticles in a block copolymer[11] and reduction in mesoporous silica.[12,13] Other platinum and palladium nanostructures have been achieved by radiolytic[14] or chemical metal reduction in soft templates.[15,16,17] Previous approaches have lacked a combination of high pore density and scalability. We present a convenient pathway to both, resulting in Pd and Pt nanopowders with 2-3 nm pores that we have produced in gram-scale batches.

5.1. Experimental

Materials: Palladium black, Ammonium tetrachloropalladate, ammonium tetrachloroplatinate, and palladium(II) chloride were purchased from Alfa. Brij 56, sodium chloride, ammonium chloride, ascorbic acid, hydrochloric acid, and ammonium hydroxide were purchased from Aldrich. All materials were used as received. 18 MΩ deionized water was prepared in the laboratory.

Metal salt paste: 17.7 mg palladium(II) chloride (0.1 mmol) and 47.0 mg sodium chloride (0.8 mmol) were added to 0.4 mL water and heated to 80 °C in a water bath. All solids dissolved, forming a brown solution. Alternatively, 28.4 mg ammonium tetrachloropalladate was dissolved in the same volume of water, with no added sodium chloride, and heated to 80 °C. For platinum, 37.3 mg ammonium tetrachloroplatinate was dissolved in 0.3 mL water and 1 mL 4M hydrochloric acid, and heated to 80 °C. 0.66 mL Brij 56, previously melted in the water bath, was added to the solution and vortexed, forming an inhomogeneous brown paste. The paste was returned to the water bath until the paste clarified to a brown viscous liquid, and vortexed again. After a third iteration of this, the paste was left on the bench to cool to room temperature, and then placed in a -20 °C freezer.

Reducing paste: 14.4 μL concentrated ammonium hydroxide (about 30%, 0.214 mmol) and 41.91 mg ascorbic acid (0.238 mmol) were dissolved in 0.186 mL water, and heated to 80 °C. 0.33 mL Brij 56 was added, and the mixture homogenized and cooled as above, resulting in a white paste.

Porous metal particles: Pastes cooled to -20 °C were kneaded together with ceramic spatulas for several minutes in a casserole dish that had also been cooled to -20 °C. No color change is seen at this point. Equal amounts of the paste were loaded into two 50 mL centrifuge tubes and returned to the freezer. One day later, the tubes were moved to a 4 °C refrigerator, and left for 2 days. The pastes were stirred and then left for 1 day at room temperature, and gradually turned

black over these 4 days. In the case of platinum, no cooling below room temperature was necessary, and the preferred reaction time was two weeks.

To remove the surfactant and byproducts, the tubes were filled with ethanol and heated to 80 °C with intermittent vortexing and sonication. This dissolved the paste, leaving a black suspension. Solids were separated by centrifugation at 6000 rpm, and the faintly yellow supernatant was decanted. The black material was resuspended in 50 mL water, heated to 80 °C for 10 minutes, and centrifuged again. The material easily resuspends in water, so it was decanted carefully, leaving approximately 1 mL. This step was repeated one more time with ethanol. The procedure has been tested on scales ranging from 0.1 mmol to 5.5 mmol. We have been able to purify up to 1 mmol per centrifuge tube.

Characterization: Transmission electron microscopy (TEM) was performed on a JEOL 2010F microscope in both TEM and scanning transmission electron microscope (STEM) modes. The electron tomography was performed in STEM mode, collecting images at tilt angles ranging from -72° to +64°, every 2°. The images were reconstructed using the simultaneous iterative reconstruction technique (SIRT) and visualized using the Amira software. Thermogravimetric analysis (TGA) was performed on a Mettler TGA100 analyzer under 20 mL/min streams of argon or air at heating rates of 1 to 10 degrees per minute. Auger electron spectroscopy was performed on a Physical Electronics 680 scanning Auger spectrometer. Auger scans were taken using a 5 keV 18 nA electron beam, averaged over a 100 x 100 μm area.

5.2. Results and Discussion

Use of hexagonal Brij 56-water mesophases as a template for nanoporous group 10 metals was developed at the University of Southampton[2] for thin films, and in bulk by Yamauchi et al.[8] This surfactant is oligo(ethylene oxide) hexadecyl ether, consisting of a distribution of oligomers that include an average of about 8 monomers. Improvements in phase behavior and other properties are seen if pure octa(ethylene oxide) hexadecyl ether is used,[3] but this material is orders of magnitude more expensive than Brij 56, which can result in highly regular pores.[10] We have attempted to use other Brij surfactants with varying ethylene oxide and hydrocarbon chain lengths, and confirmed that Brij 56 is the best route to regular pores.

We followed Yamauchi's lead in the use of a chemical reducing agent blended with a metal salt. This approach is more scalable than multiphase methods such as reaction at a planar electrode, and is accessible at the near-room temperature conditions in which the surfactant-water mesophase is stable. This and the need to homogenize the paste at elevated temperature make thermolytic approaches unfeasible. In the case of platinum and palladium, however, the borohydride reducing agents used by Yamauchi are much more potent than necessary. It is desirable to perform a slow reaction that minimizes concentration gradients in the paste that could disturb the structure of the surfactant. Use of borohydride reductants with metals results in metal boride impurities, which can affect material properties in unwanted ways.[8] We found that the tetrachloro complexes of palladium and platinum can react at moderate rates with ascorbic acid, and that the reaction rate is tunable with temperature, chloride concentration, and pH. The palladium salt is stable in the heated paste, but this is only true for platinum under acidic conditions. At higher pH, a control experiment with ethylene glycol dimethyl ether suggests that

the platinum salt can oxidize the oligo(ethylene glycol) backbone, reducing itself to the metal, before the paste is properly homogenized. This reaction does not strongly depend on chloride concentration.

The reaction of ascorbate with the metal salts yields a proton, taken up here by another ascorbate anion, and dehydroascorbate, which exists in an acetal form under our conditions.[18,19] The pH in the described reaction is designed to start at about 5 and end at about 3.2 (the pKa is 4.2 and the reaction should proceed from about 90% ascorbate to 90% ascorbic, consuming 1 mmol ascorbate in the process). When the reaction is performed in D_2O and the byproducts observed by NMR, we found a 2:1 superposition of the known spectra of ring-closed dehydroascorbate and ascorbic acid, with only traces of ascorbate anion, so some excess oxidation is occurring. Because the reaction rate is tunable using chloride, we expect that ascorbate competitively coordinates with the metal salt as an initial step of the reaction. While ascorbate complexes of palladium have not been isolated, platinum complexes likely to be similar are known.[20] We found that particle morphology was not highly sensitive to the pH and amount of excess ascorbate, but these values allow the reaction to proceed to completion at a rapid and uniform rate, avoiding unreacted brown Pd salt in the supernatant.

At room temperature, mixing the palladium and ascorbate pastes results in immediate reaction; the mixture turns gray or black in patches. It is preferable to slow the reaction so that it does not occur on the timescale of mixing and that microscopic conditions are as uniform as possible. Adding 8 equivalents of sodium or ammonium chloride to the palladium paste (or 6 to the Pd paste and 3 to the ascorbate paste) slows the reaction rate sufficiently. This can also be achieved by reducing temperature. The results reported here use both approaches. It is preferable to use primarily the latter, because it results in less material that must be removed during the isolation steps. The reaction is exothermic, so care must be taken during mixing to keep the temperature low. For scales much larger than 1 gram, use of chloride to slow the reaction may be preferable, but we obtained satisfactory results by kneading on a cold, nonporous surface.

Cleaning the product is challenging given the high surface area, pore aspect ratio, and reactivity of a bare Pd surface. Figure 5.1 shows thermogravimetric analysis of a Pd product sample performed under argon and air.

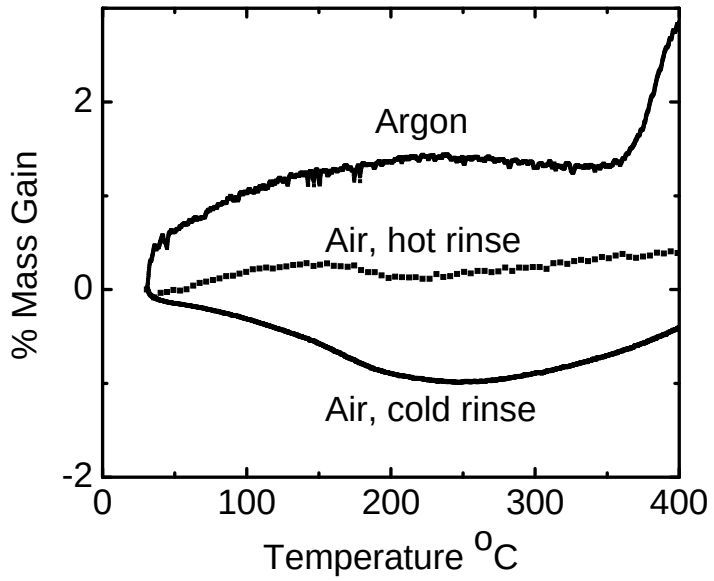

Figure 5.1. TGA of nanoporous palladium in argon (10 K/min) and air rinsed in room temperature (1 K/min) and heated ethanol (2 K/min).

No mass loss occurs under argon, but changes in the 1% range are seen under air at 180-200 °C, suggesting the presence of organic contaminants. This number is several times smaller if the washing steps are heated as shown in the middle curve of Figure 5.1. Unlike the two air curves, the argon curve was not corrected for background effects which are the likely cause of the significant mass gain shown in Figure 5.1. If the water wash is omitted, sodium, chloride, and carbon peaks appear in the Auger spectrum, but these are strongly diminished after washing, as shown in Figure 5.2. As a reference point, if pores are assumed to be spaced by one diameter, one would expect about 20% of the material's volume to be pores, and palladium is 10 times denser than typical organic material, so clogged pores would be expected to show a 2% mass loss in the air analysis.

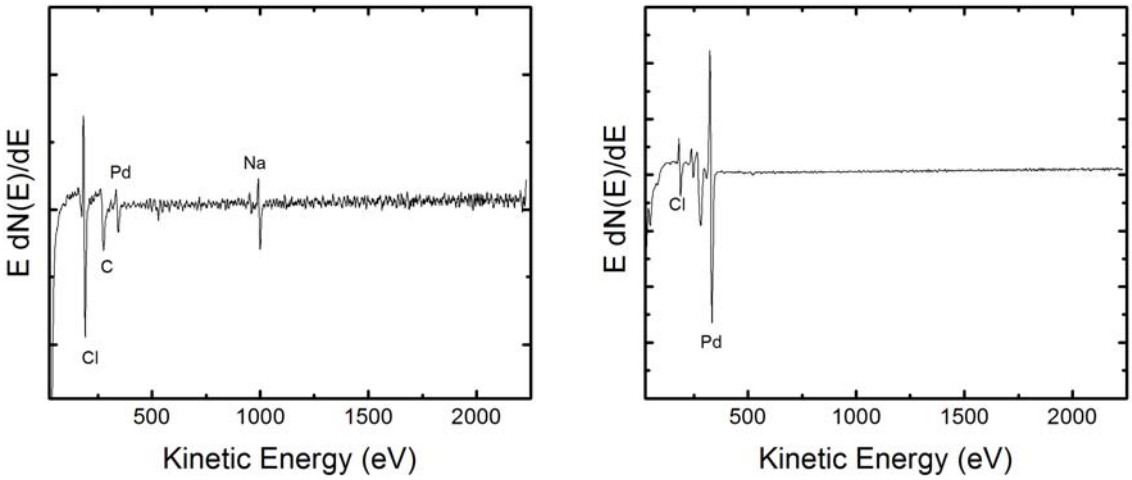

Figure 5.2. Auger spectrum of palladium sample (left) washed in ethanol and (right) washed with ethanol, then water, and then ethanol.

Pore geometry can be elucidated using transmission electron microscopy and tomography. Figure 5.3 shows particles imaged at zero tilt angle, showing faceted particles in the 50 nm range that are perforated by 2-3 nm pores arranged with a degree of regularity and density but not close-packed.

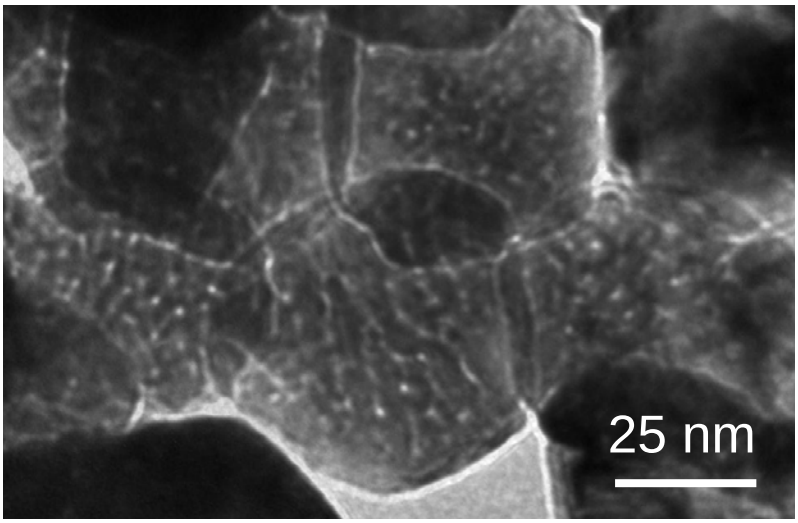

Figure 5.3. TEM image of nanoporous palladium

To demonstrate that the high-contrast regions are pores that go through the entire particle, scanning transmission electron micrographs were collected at many angles and reconstructed to form a three-dimensional representation of several particles. Slices through this are shown in Figure 5.4, showing pores that run the length of the particle, with slight irregularities in their path.

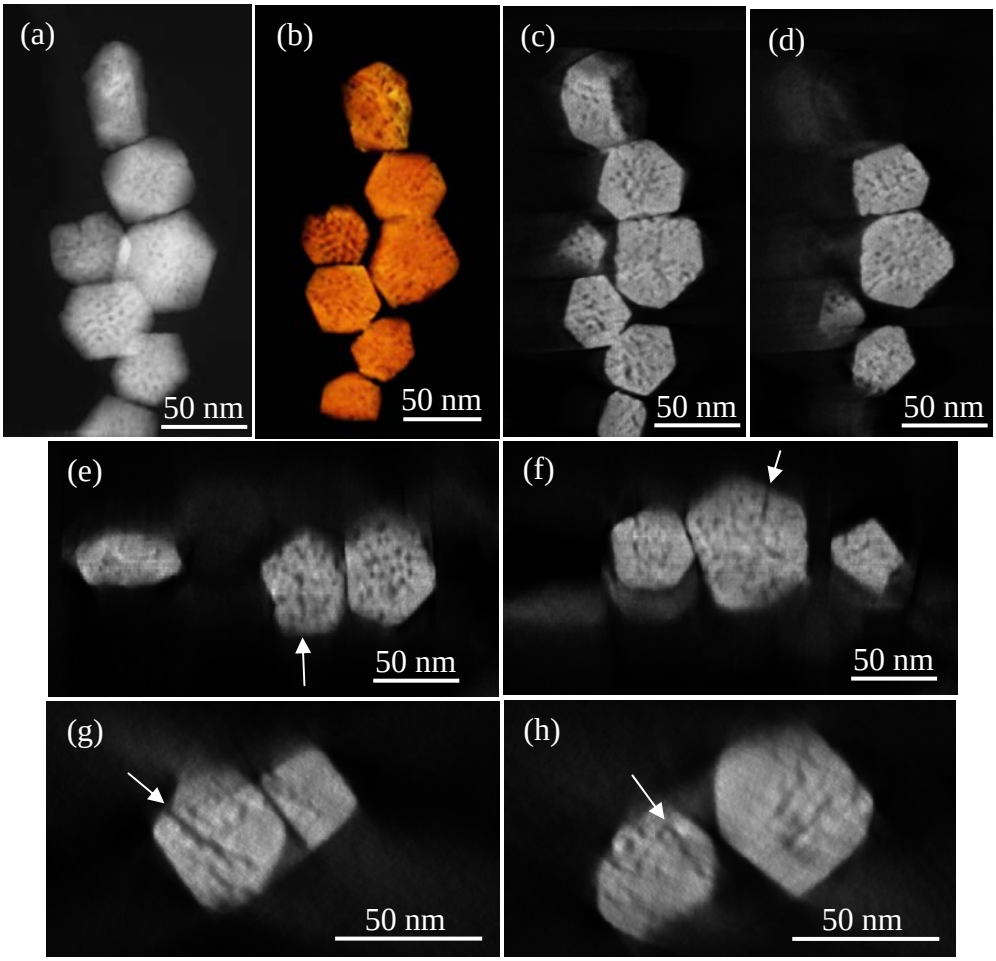

Figure 5.4. 3-D reconstruction of a set of porous Pd particles. (a) shows one of the original STEM images from the tilt series. (b) shows the 3-D reconstruction volume rendered. (c)-(d) show 1nm-thick slices through the reconstruction in the orientation of (b). (e)-(f) show slices through the reconstruction in an orientation perpendicular to (b) (from the right to left of (b)). (g)-(h) show slices through the reconstruction from the top to bottom of the particles seen in (b). Arrows indicate regions where some pores are extended in length, but all of the slices demonstrate the porosity is tortuous and extends throughout the particles in all directions.

Figure 5.5 shows a micrograph of platinum particles produced by the procedure described in the experimental section, showing a greater degree of pore regularity. Palladium produced under the more acidic conditions used for platinum looks essentially the same as Figure 5.3.

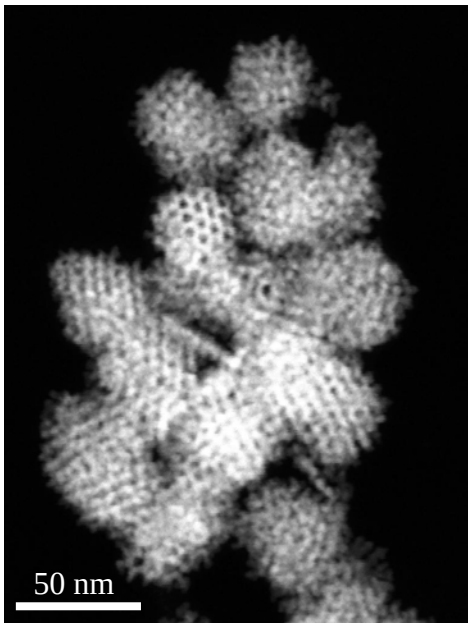

Figure 5.5. STEM image of nanoporous platinum

Electroplated palladium in purified surfactant shows regular pores,[3] but the more constrained environment of a film may make regularity easier to maintain than in a free particle. We suspect that the surfactant assembly is perturbed by concentration gradients of reactants and products, which are exacerbated by higher reaction rates, and that specific interactions between the particle surface and the products or surfactants influence structure; these are possible explanations for the differences observed.

The material presented here is easy to prepare and is of potential benefit to hydrogen storage, electrical energy storage, and catalysis applications due to the high exposed surface area provided by a high density of pores. The pores are small enough that thermal stability of the particles is a concern; high pore surface energy may result in their collapse at low temperatures. Results reported here show that the 2-3 nm pores reported here are stable at 80 °C in liquids and at 150 °C under vacuum, but pores much smaller than this may not be; we hypothesize that Brij 56 templates may result in the highest practical surface areas for porous metals. We are currently studying the thermal, electrical, and hydrogen-related properties of these materials to determine their utility for energy storage and conversion.

5.3. Surfactant Templating References

[1] Lewis, F. A. *International Journal of Hydrogen Energy* **1996**, *21*, 461.

[2] Attard, G. S.; Bartlett, P. N.; Coleman, N. R. B.; Elliott, J. M.; Owen, J. R.; Wang, J. H. *Science* **1997**, *278*, 838.

[3] Bartlett, P. N.; Gollas, B.; Guerin, S.; Marwan, J. *Physical Chemistry Chemical Physics* **2002**, *4*, 3835.

[4] Choi, K. S.; McFarland, E. W.; Stucky, G. D. *Advanced Materials* **2003**, *15*, 2018.

[5] Denuault, G.; Milhano, C.; Pletcher, D. *Physical Chemistry Chemical Physics* **2005**, *7*, 3545.

[6] Elliott, J. M.; Attard, G. S.; Bartlett, P. N.; Coleman, N. R. B.; Merckel, D. A. S.; Owen, J. R. *Chemistry of Materials* **1999**, *11*, 3602.

[7] Elliott, J. M.; Owen, J. R. *Physical Chemistry Chemical Physics* **2000**, *2*, 5653.

[8] Yamauchi, Y.; Momma, T.; Yokoshima, T.; Kuroda, K.; Osaka, T. *Journal of Materials Chemistry* **2005**, *15*, 1987.

[9] Yamauchi, Y.; Yokoshima, T.; Momma, T.; Osaka, T.; Kuroda, K. *Journal of Materials Chemistry* **2004**, *14*, 2935.

[10] Yamauchi, Y.; Yokoshima, T.; Momma, T.; Osaka, T.; Kuroda, K. *Electrochemical and Solid State Letters* **2005**, *8*, C141.

[11] Warren, S. C.; Messina, L. C.; Slaughter, L. S.; Kamperman, M.; Zhou, Q.; Gruner, S. M.; DiSalvo, F. J.; Wiesner, U. *Science* **2008**, *320*, 1748.

[12] Shin, H. J.; Ko, C. H.; Ryoo, R. *Journal of Materials Chemistry* **2001**, *11*, 260.

[13] Kang, H.; Jun, Y.; Park, J. I.; Lee, K. B.; Cheon, J. *Chemistry of Materials* **2000**, *12*, 3530.

[14] Surendran, G.; Ramos, L.; Pansu, B.; Prouzet, E.; Beaunier, P.; Audonnet, F.; Remita, H. *Chemistry of Materials* **2007**, *19*, 5045.

[15] Kijima, T.; Yoshimura, T.; Uota, M.; Ikeda, T.; Fujikawa, D.; Mouri, S.; Uoyama, S. *Angewandte Chemie-International Edition* **2004**, *43*, 228.

[16] Solla-Gullon, J.; Montiel, V.; Aldaz, A.; Clavilier, J. *Journal of the Electrochemical Society* **2003**, *150*, E104.

[17] Teng, X. W.; Liang, X. Y.; Maksimuk, S.; Yang, H. *Small* **2006**, *2*, 249.

[18] *Ascorbic acid : chemistry, metabolism, and uses*; Seib, P. A., Tolbert, B. M., Eds.; American Chemical Society: 180th ACS National Meeting, Las Vegas, Nevada, 1980.

[19] Kurata, T.; Nishikawa, Y. *Bioscience, Biotechnology, and Biochemistry* **2000**, *64*, 1651.

[20] Arendse, M. J.; Anderson, G. K.; Rath, N. P. *Inorganic Chemistry* **1999**, *38*, 5864.

6. Helium Release Measurements

A new tritium manifold was constructed to measure the Early He Release Fraction (ERF) from tritiated materials. A schematic diagram of the apparatus is shown in Fig. 6.1. Six 6.9 cc sample holders are mounted symmetrically around a hexagonal 6-port fitting (Hex) which leads to common tritiding and gas analysis systems. During aging each sample is continually supplied with purified tritium gas through individual, heated Pd-foil filters (Pd). While sample tritiding and aging temperatures can be individually selected, the samples will initially be tritided as a group using a controlled leak valve (LK) and leak bypass valve (LB). At prescribed aging intervals, the gas atmosphere over each sample will be examined by closing the sample S-valve and momentarily opening its alloquat A-valve to the common Hex and gas analysis system. Here, the expanded total gas pressure will be determined by coarse (PD) and fine (Baro) pressure gauges. The tritium fraction within this alloquat will then be gettered through (GP) using a small getter pump, leaving the He overpressure which will be measured by the Baro. After each sample has been cycled through the measurement sequence, the Hex valve (HX) will be closed and the getter desorbed to the tritium recovery system and LLNL manifold. Sample S-valves will be opened after the alloquat volumes (Va) have been sufficiently re-supplied with tritium through the Pd filters, as determined by monitoring the upstream pressure (PU) drop. In this fashion samples will never be exposed to the pressure transients that modify He bubble development.

An ERF simulation code was generated to examine the measurement sensitivities and uncertainties for this apparatus. It simulates the helium and tritium pressure changes within each sample holder and measurement volume and allows exploration of the effects of component temperature changes. An example of the code output (Fig. 6.2) shows how the measured He pressure is expected to change with time for six samples aging at room temperature, each with a constant ERF prescribed by the material's structure and nucleation temperature (temperature during the first few days following tritiding).

The ERF Manifold has been installed into the new Tritium Science Station (TSS) glove box at LLNL, which is currently undergoing final tritium operations approvals from NNSA. The ERF experiment has received high priority and is scheduled to see first tritium exposure this fall.

Characterization of commercial palladium black: Palladium black was obtained from Sigma-Aldrich (S-A No. 205834). The quoted surface area for this material is 40-60 m^2/gm, corresponding to an average spherical particle diameter of 12.5 to 8.3 nm. TEM micrographs found it to be composed of clusters of particles of 7-17 nm diameter. (Fig. 6.3)

Hydrogen pressure composition isotherms (PcT) were obtained on a 1 gram quantity this material and are shown in Fig. 6.4. The sample was pretreated with two cycles of absorption/desorption prior to measurement. Isotherms were measured for both absorption and desorption at 100 and 200 C and for absorption at 23 C. Desorption at 23 C was not measured due to its low desorption pressure. The results are very close to those reported in the literature for bulk Pd, shown as Wicke in this figure. [Wicke 78] These authors point out the differences between bulk Pd and Pd black are (a) a smaller hysteresis for Pd black due to its higher desorption pressure and (b) a small shift toward larger H/Pd due to a higher stoichiometry (near

unity) for surface sites. This lattershift is not found in our measurements perhaps due to incomplete removal of H, which requires 500 C or above [Kubicka 66].

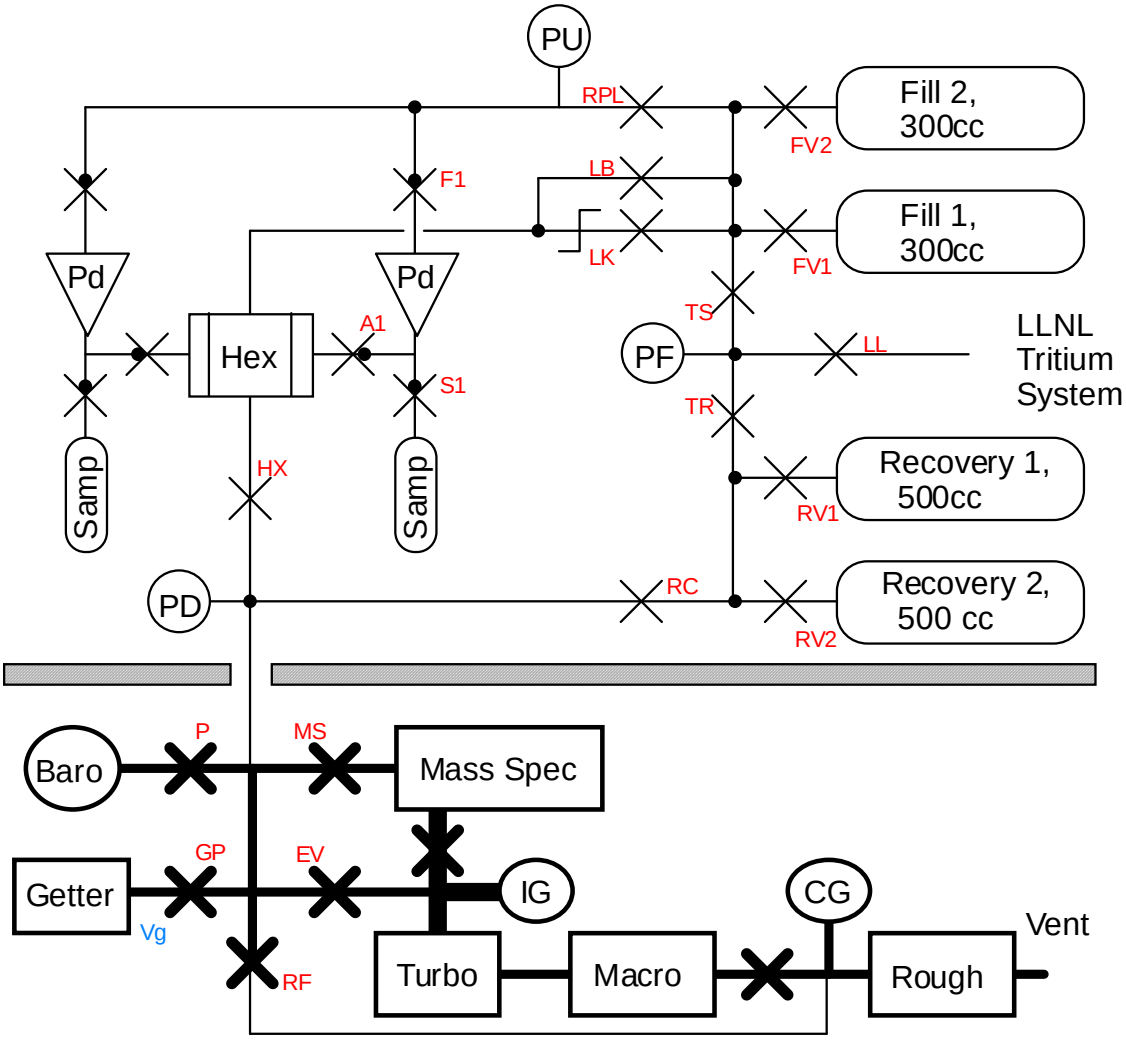

Figure 6.1. Early Release Experiment (ERX) tritium manifold for measuring the Early He Release Fraction (ERF).

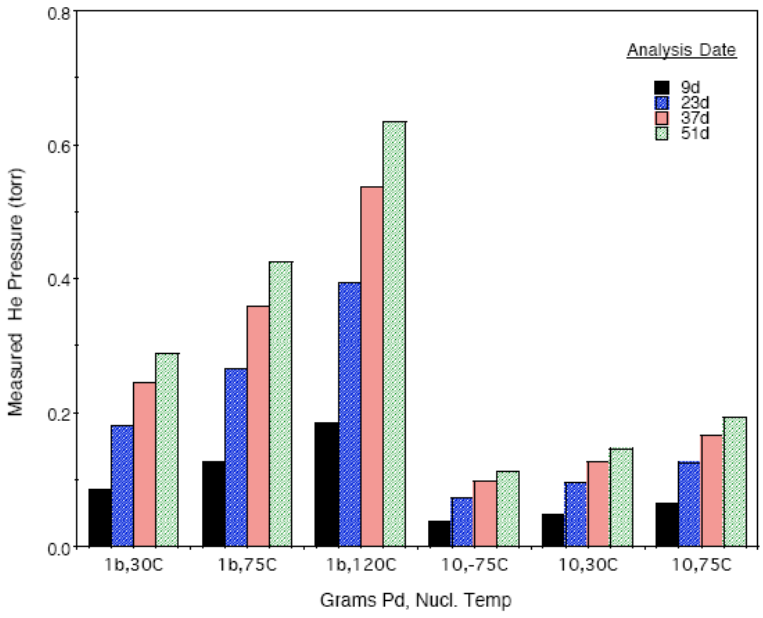

Figure 6.2. Measured He pressure for three 1 gm samples of Pd black and three 10 gm samples of fine Pd powder exposed to selected nucleation temperatures, as calculated using the ERXsim code.

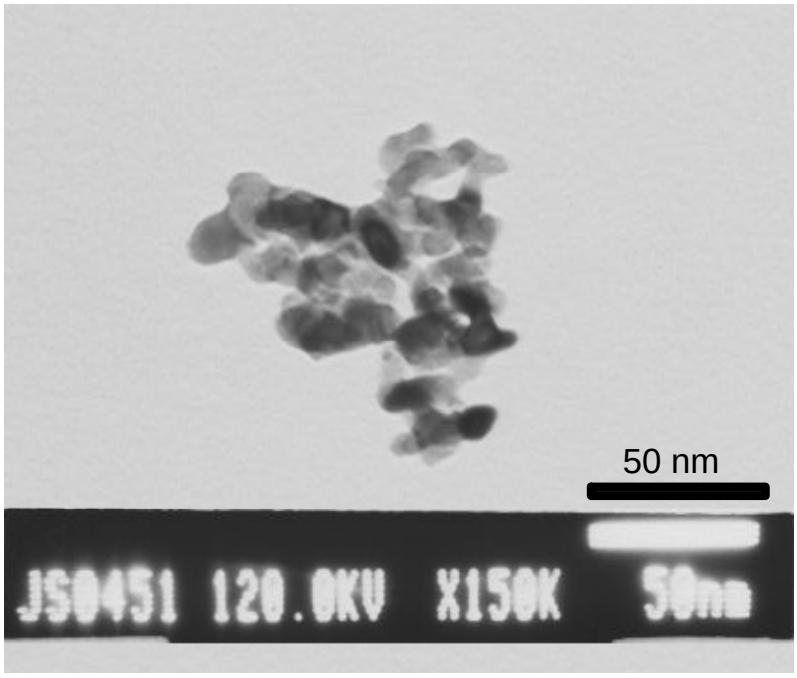

Figure 6.3. TEM micrograph of Sigma Aldrich palladium black showing a cluster of particles with 7-17 nm diameter.

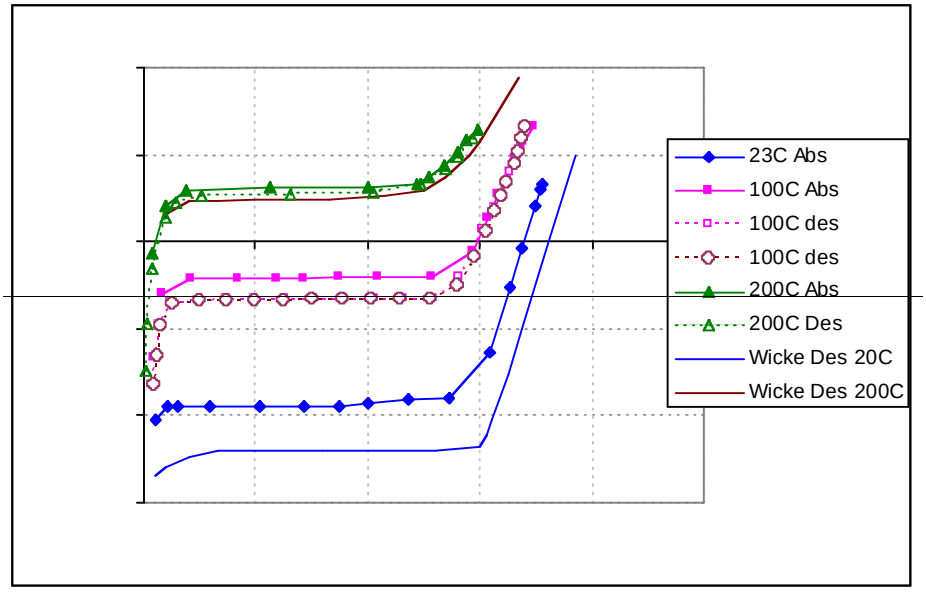

Figure 6.4. Measured hydrogen absorption and desorption isotherms for Sigma Aldrich palladium black.

7. Conclusions and Proposed Next Steps

From the beginning, it was recognized that this 1-year investigation would be far too short to provide a meaningful determination of the potential of nanomaterials for He-free storage of tritium. We did, however, achieve several significant steps toward this goal. The SBE code was adapted to nanomaterial and is generating useful predictions of the effects of ligament dimension and temperature on He retention. It also provides information on the effects of temperature and tritium pressure changes during aging. The uncertainty in these predictions is expected to improve as more reliable He diffusion and trapping parameters become available.

A successful synthesis pathway was identified for creating for nano-structured palladium powders. A surfactant templating process was created which generated 50 nm Pd powder particles with 2-3 nm pore structures. Several processes were examined for removing solvent residue from the pores, but additional work is needed in this area. The stability of the pore structures in a hydrogen atmosphere at elevated temperatures needs further examination. Additional efforts will also be needed to increase the material's density. The process, however, should be sufficiently scalable for generating large batches of material.

Free corrosion de-alloying of PdAg alloys using a piranha solutions was also successful in creating nano-Pd. It is likely that material with the desired morphology can be generated by fine-tuning the process. The results obtained with this and several other alloy-etchant combinations, including some experience with electro-corrosion processes, are documented in this report. This information will provide a useful starting point for additional study.

Lastly, we provide a short description of the early He release apparatus created for characterizing He retention in nanomaterials and for quantifying the effect of bubble nucleation temperature in standard materials. An experiment simulation code (ERXsim) was created to examine experimental sensitivities to various materials, conditions, and uncertainties. A more complete description of this apparatus and the ERXsim code will be given in a future publication documenting the results of actual measurements.

Distribution:

1	MS0899	Technical Library, 9536 (electronic copy)
1	MS0123	D. Chavez, LDRD Office, 1010


Sandia National Laboratories